Passive Probe: Mechanically-Modulated Field Sensing for Motion Tracking and Flow Estimation

Eric A. Ponce and Steven B. Leeb, *Fellow, IEEE*

***Abstract*—The internal mechanical motions of a dynamic system can serve as the basis for developing "free" sensors that probe operating state and potentially diagnostic health. Specifically, the interaction of a moving mechanical structure with an applied, nonintrusive field, e.g., an electric or magnetic field, can produce a signal that creates a sensor with little additional hardware. In this paper, bellows-and-diaphragm natural gas (BDNG) meters provide an illustrative example for three different approaches for transforming a metering mechanism and its consumption totalizer into a high quality flow meter. Detailed flow information provides a data-stream for nonintrusively monitoring the real-time operation of loads – in this example case, loads that consume natural gas such as burners, heaters, and engines. The flow information can also be used for fault detection and diagnostics, e.g., for finding leaks or correlating faulted operation with respect to the operation of electrical actuators or other flows of consumables like water. This paper examines three BDNG meters and presents a methodology for inexpensively adding digital flow-rate measurement capabilities to each meter. The methods developed here can in principle be applied to any dynamic machine for consumption estimation or fault detection. They can also be used with other nonintrusive field stimuli including light and sound. Mechanical retrofit techniques are described, and exemplary signal processing and estimation chains including compensation, flow rate estimation, and post processing are presented.**

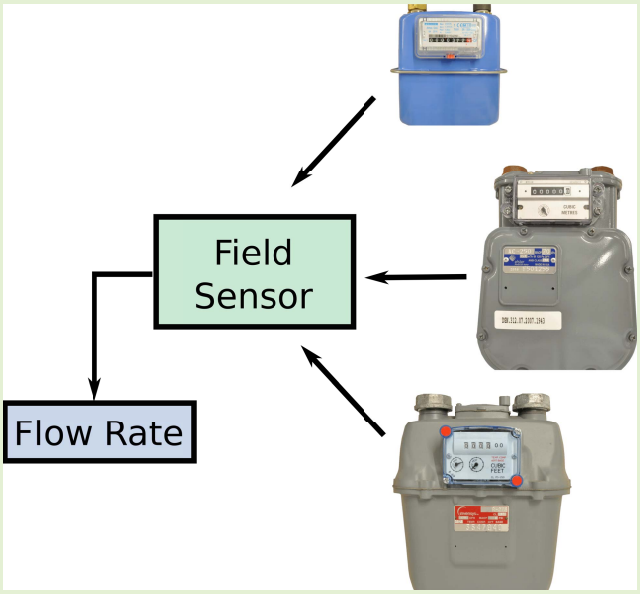

***Index Terms*—Fluid flow measurement, magnetic sensors, sensor data processing, sensor applications.**

I. Introduction

INTERNAL motions of a dynamic system reveal details about the system's operation. These motions can help track or totalize use. Deviations in these motions can be used to detect faults or pathologies in the system. Tracking motion is a time-honored technique for creating meters or "odometers" for a variety of systems. When a mechanical system's own motions can be sensed with a field or nonintrusive probe, an opportunity exists to create a hybrid system that can provide indications of usage and operation. This hybrid lets a mechanism serve a "dual-use" for monitoring. This approach also enables nonintrusive or low intrusion monitoring that avoids unneeded sensors and that can provide useful redundancy for existing sensors. Non-intrusive approaches make better use of fewer sensors, enabling an easier road to automated smart control systems and metering, distributed management for improved reliability and efficiency of electromechanical systems, and improved monitoring in resource-constrained environments [1].

A simple approach for exploiting motion detection for sensing takes advantage of serendipitous, nonintrusive field sources. This, for example, is the underlying approach for a non-contact tachometer. Reflection of light off a moving surface with contrast variation can create a detectable signal for measuring rotations or other motion. Other systems may offer an inherent field emitter. For example, water meters that totalize consumption are sometimes designed with a moving magnet that provides a noncontact rotary coupling to a gear box in the meter totalizer. The moving magnet creates field signals that can be probed nonintrusively. Variation in the position of, and flow through, a positive-displacement cup can be extracted with a combination of analog sensing and digital signal processing to reconstruct finely detailed, high resolution flow estimates in real-time [2], [3].

Manuscript received October 22, 2021; accepted December 29, 2021. Date of publication January 14, 2022; date of current version February 28, 2022. This work was supported in part by The Grainger Foundation and in part by Exelon Corporation. The associate editor coordinating the review of this article and approving it for publication was Dr. Wei Wang. *(Corresponding author: Eric A. Ponce.)*

The authors are with the Department of Electrical Engineering and Computer Science, Massachusetts Institute of Technology, Cambridge, MA 02139 USA (e-mail: eaponce@mit.edu; sbleeb@mit.edu).

Digital Object Identifier 10.1109/JSEN.2022.3143430

(a) (b) (c)

Fig. 1. Type I (a), Type II-A (b), and Type II-B (c) BDNG meters explored in this study.

Bellows-and-diaphragm natural gas (BDNG) meters are another example of a mechanical metering totalizer with untapped potential as a flow meter. The totalizer on many existing BDNG meters can already be retrofit with pulse outputs for digitizing meter output. These pulse outputs lack resolution at low flow rates, providing one pulse per several cycles of the internal counting mechanism. Nevertheless, past research has used these pulse-output attachments on specifically selected high-sensitivity meters for successfully disaggregating load profiles downstream from the meter [4], indicating the potential value of flow information from retrofit systems. Another method for retrofitting BDNG meters involves modifying the meter by replacing the counting mechanism with a high-resolution device to measure flow rates, also with the aim of disaggregation of loads [5]–[7]. This paper presents approaches that avoid permanent physical alteration of the meter. These approaches can therefore be adapted to many other moving mechanical systems for use-tracking and diagnostics.

Dynamic systems with "buried" or hidden motions and no inherent field source can be probed with the addition of a passive, external field source that becomes modulated by the system motion. This paper illustrates this approach using BDNG meters as a target, converting these meters into real-time flow sensors with three different retrofit techniques. Like water meters, these BDNG meters are placed upstream from residential, commercial, or industrial gas loads. Projected increases in the use of natural gas as a replacement for coal [8] have lead to great interest in detecting gas leaks at the source and in the supply chain using various sensors and machine learning [9]. Inexpensive retrofit techniques that avoid the need for a skilled technician for installation would offer a relatively low-cost method for extracting detailed real-time flow information. Harnessing the underutilized information that can be extracted from mechanical devices like these meters adds value and the possibility for creating "smart" systems out of existing dynamic machines.

The three retrofit techniques are illustrated in the following sections. First, existing magnetic field sources inherent in some BDNG meters are exploited to create nonintrusive retrofits for detecting flow. Second, BDNG meters with internal ferromagnetic components are probed using an external magnetic field to detect cycling. Third, BDNG meters with dielectric (plastic) internal construction are probed using an externally applied electric field to detect internal motion. In all cases, flow can be extracted or recovered from the detected signals, and the examples here serve as guides for probing other moving mechanical devices.

II. Opportunity

Bellows-and-diaphragm natural gas meters primarily consist of a diaphragm mechanism for inflating and deflating a set of bellows designed to measure a fixed volume of gas flowing through the body of the meter. A coupler connects the meter body (MB) to a tamper-resistant meter index (MI) designed to accumulate, or totalize, the flow of gas for tracking and billing purposes. The coupler generally comes in the form of a sealed mechanical or magnetic coupler. The bellows act as expandable lungs, taking gas up to a known, fixed volume, and then expelling it down-stream into the network for each cycle. The diaphragm uses a system of valves and linkages to control the alternating filling and emptying cycles. As these linkages move, they rotate the coupler to register gas flow with the MI [5], [10]. The presence of two bellow compartments requires them to move out of phase with one another such that the bellow cycles are out of phase by one quarter cycle.

These meters come in many different shapes and sizes, depending on the downstream load. The pressurized bodies of older and smaller residential meters are generally constructed of steel or cast iron, whereas larger residential meters can be constructed from cast or molded aluminum [11]. The sections below describe the mechanical properties of two types of meters that prove useful for flow rate extraction purposes.

A. Type I Meter

A BDNG meter sized for apartment-sized units [12] shown in Fig. 1a is composed of a two-part steel MB with each half separated by an insulating sealant and clamped to the other with a metal band. The MB contains a plastic bellows-and-diaphragm mechanism. The MI is coupled to the MB through a two pole-pair diametrically-polarized cylindrical magnetic coupler and contains two smaller magnets on the index wheel

for use with commercially available pulse-output attachments. The magnetic coupler revolves once per cycle of the bellows, which corresponds to $1.19\,\mathrm{dm}^3$ of gas. One revolution of the index wheel corresponds to $28.3\,\mathrm{dm}^3$ of gas and one output pulse [12]. Thus, available pulse-output attachments will produce one output pulse for approximately 24 cycles of the bellows and revolutions of the internal magnetic coupler.

For this specific meter, the magnetic coupler produces a magnetic field that may be measured to sense this internal motion. A diametrically-polarized magnetic disk field solution [13] may be used to model the field produced by this coupler and will show the presence of orthogonal field components that form a quadrature signal, as well as two sinusoidal periods per revolution of the coupler due to the number of pole-pairs. The two cycles of the fundamental harmonic of the field per revolution of the coupler leads to approximately 48 periods of sinusoidal data per single equivalent output pulse. This results in a much higher possible volumetric resolution when using the field to probe the internal motion of the counting mechanism, especially when sampling at frequencies high enough to record multiple points of data per fundamental field period. Due to the high-permeability steel MB, and an inner magnet that diverges considerably from the standard geometric model, however, the field for this specific meter was not computed. The high-permeability material case, in particular, requires more careful magnetic image analysis to compensate for the boundary conditions introduced by the steel. Nevertheless, a measurement point that aligns a field sensor's Cartesian axes with the coupler's cylindrical axis can be found and the orthogonal field components and 2:1 ratio of field fundamental to mechanical revolution still holds.

For meters of a similar construction but using a non-magnetic coupler, the insulating sealant between two conductive metal halves of the MB provides an opportunity to apply a weak electric field internal to the meter for probing its motion. Applying a voltage across this insulating boundary induces an electric field through a space containing a dielectric plastic mechanism, the bellows-and-diaphragm, whose configuration changes as it cycles. These moving parts will, in a sense, change the effective permittivity of this space as gas flows through the meter. For experimental and safety purposes, we used compressed air for testing these permittivity based flow rate extraction techniques. Since the relative dielectric constant of most gases is nearly one, which is low compared to the plastic bellows-and-diaphragm mechanism, we do not expect drastic changes to performance in the presence of different gas compounds.

B. Type II Meter

The second type of BDNG meter explored in this work is designed for larger residential natural gas service. The first type II meter explored, a *Honeywell-Elster* AC-250 Residential Diaphragm Meter [14], is shown in Fig. 1b and will be referred to as the Type II-A BDNG Meter. The second type II meter, a *Sensus* R-275 Residential Diaphragm Meter [15], is shown in Fig. 1c and will be referred to as the Type II-B BDNG Meter. Both examples target the same type of load, have a MB composed of low-permeability aluminum, and do not contain magnetic couplers as in the Type I BDNG meter. They also contain high-permeability steel flag rods connecting the outer end of the bellows to the diaphragm control mechanism. As the bellows expand and contact, the portion of the flag rod connected to the bellow moves closer and farther from the outer wall of the MB.

A magnetic field may be applied near the rotary axes of these flag rods from the exterior of the MB to passively probe the meter's motion. Flux will be coupled to the arm end of the rod that mounts to the center the bellow. Thus, the strength of the field at the exterior point near the center of the bellow will vary as the meter cycles. Each period of the measured field strength will correspond to one cycle of the bellows. The meters have a cyclic volume of $3.125\,\mathrm{dm}^3$ and $3.53\,\mathrm{dm}^3$ for Type II-A and Type II-B, respectively. Using two sensors, one near each bellow, one can generate a set of orthogonal sinusoids for flow-rate extraction processing. Due to the non-ideal approach taken, the measured fields will be non-linear and will contain large harmonic components over a cycle of the bellows. These non-linearities and harmonics will be compensated for with signal processing techniques presented below.

III. Sensing Hardware and Signal Preprocessing

A. Magnetic Field Sensor and Measurement Setup

A three-axis Hall effect (HE) sensor integrated circuit, the MLX90393, with built-in ADC and digital filtering by Melexis [16] was used to measure magnetic fields external to the meters. The highest resolution mode of the HE sensor was used without saturation. The sensor produces samples measuring the field in the three component directions from the center of the integrated circuit, referenced here as $\widehat{x}$, $\widehat{y}$, and $\widehat{z}$. Sensor positioning is selected and demonstrated for each of the different meters below.

1) Type I Meter: A point physically close to the internal magnetic coupler, but far from the pulse-output magnets, is chosen as the measurement point. An elastic holds the sensor against the MI as shown in Fig. 2a, illustrating the simplicity of the mechanical requirements for this retrofit.

The magnetic coupler will produce a field in the $\widehat{\theta}$ component direction of its reference frame that is orthogonal to the $\widehat{r}$ and $\widehat{z}$ components, in cylindrical coordinates. Fig. 2a shows the magnetic coupler's cylindrical basis $(\widehat{r}, \widehat{\theta}, \widehat{z})$ in red and the HE sensor's sensing directions $(\widehat{x}, \widehat{y}, \widehat{z})$ in black. In the chosen sensor position, the sensed $-\widehat{x}$ and $-\widehat{z}$ directions correspond most closely to the coupler's $\widehat{\theta}$ and $\widehat{r}$ directions, respectively, with the former component leading the latter. As such, the measured $-\widehat{x}$ and $-\widehat{z}$ components will be referred to as $\tilde{c}_i[n]$ and $\tilde{s}_i[n]$ representing the *cosine* and *sine* terms in an analytic signal $\tilde{z}_i[n] = \tilde{c}_i[n] + j\tilde{s}_i[n]$.

Analytic signals formed from quadrature, orthogonal, signals that move forward in one direction contain no negative-valued frequency content. This content serves as a valuable metric for reducing sensor misalignment. For three-axis data, there is a standard rotation matrix [17] that minimizes negative-valued frequency content in the two component directions of interest and can be found using standard minimization and optimization techniques. This served as a justification for

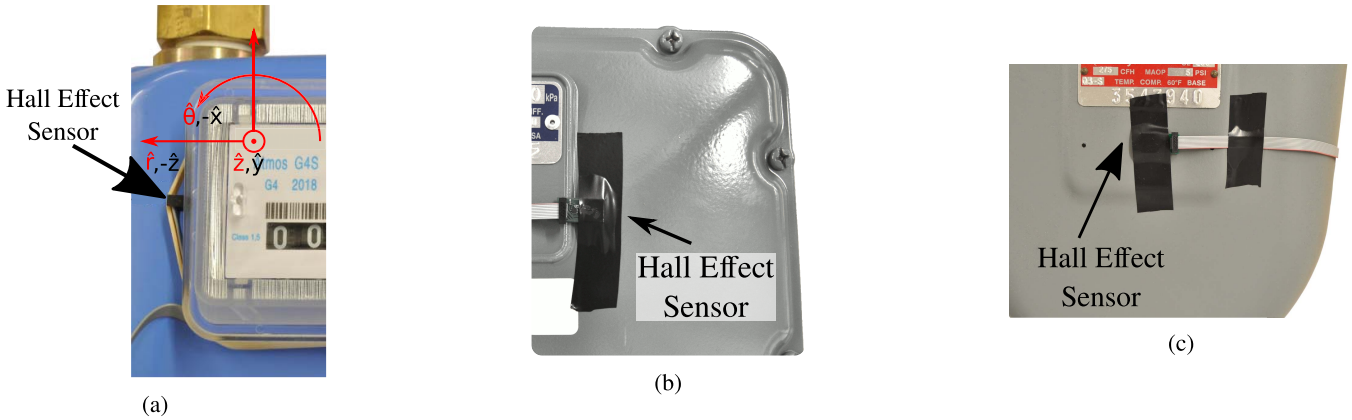

Fig. 2. Hall Effect sensor placement for Type I (a), Type II-A (b), and Type II-B (c) BDNG meters.

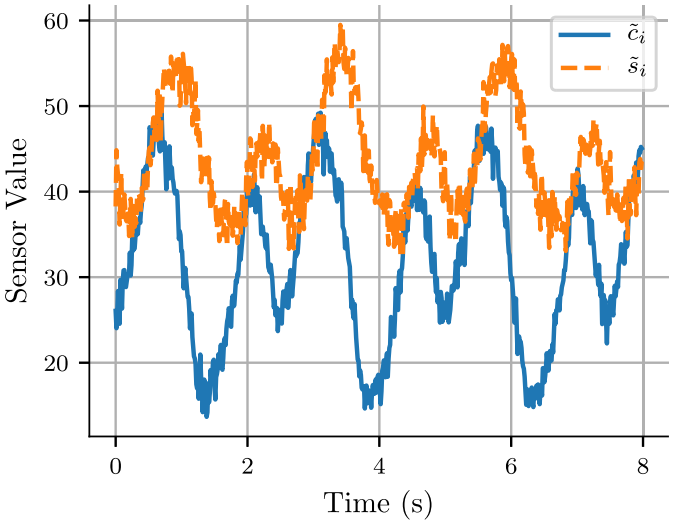

Fig. 3. Type I sample waveforms.

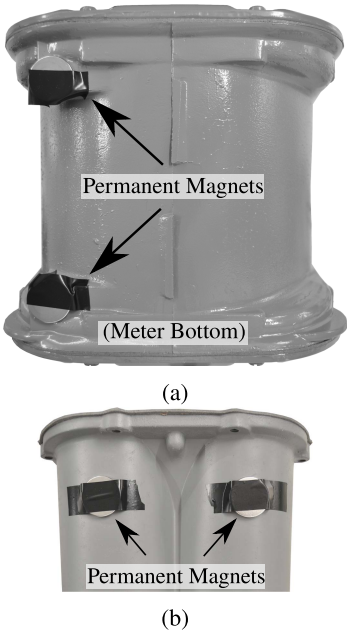

Fig. 4. Permanent magnet locations for Type II-A (a) and Type II-B (b) BDNG meters.

choosing a three-axis sensor over a two-axis sensor, loosening mechanical alignment requirements. For the sensor placement in this work, the axes were well enough aligned that this step could be skipped.

The sensor was sampled at a rate of 250 Hz. Sample waveforms for $\tilde{c}_i[n]$ and $\tilde{s}_i[n]$ are shown in Fig. 3. They demonstrate a clear harmonic at one-half of the fundamental frequency which stems from the number of pole-pairs and magnetization asymmetries in the coupler. They also show inherent offset and amplitude imbalances between the components that must be corrected for with preprocessing algorithms.

2) Type II Meters: The Type II BDNG meters do not contain inherent fields that correspond to their motion. So, an external magnetic field is applied to the meter to passively probe its motion by attaching large permanent magnets to the MB near the flag rods using an adhesive. Convenient flat sections on the bottom of the Type II-A meter where the flag rods are seated were used as shown in Fig. 4a. The Type II-B meter did not have these sections, so instead the magnets were attached to the side of the meter near rods as shown in Fig. 4b. HE sensors were affixed near the center of the bellow on each side of the meter. Sampling positions on one side of the MB are shown in Fig. 2 for both Type II meters. The meters exhibited the strongest field strength in the sensor's $\hat{x}$ and $\hat{z}$ directions for the Type II-A and II-B meters, respectively. $\tilde{c}_i[n]$ was chosen so that it would lead $\tilde{s}_i[n]$. For both meters, some care was taken to ensure that sensors on either side of the meter were symmetrically placed. Ultimately, however, the system was robust to deviations in sensor placement for distances greater than 2 cm.

The sensors were sampled at a rate of 250 Hz. Fig. 5 and Fig. 6 show sample quadrature waveform pairs from these meters, decimated by a factor of 10 for illustrative purposes. The waveforms have a reasonably high SNR but contain higher-order harmonics that distort the waveform and offset and amplitude imbalances. In particular, the Type II-B meter showed higher distortion due to larger mismatches in the placement of the permanent magnets. Nevertheless, these waveforms are periodic and sinusoidal in nature and can provide data for flow rate extraction.

Using one sensor on each side of the meter provides an opportunity for adding diagnostic capabilities. If the motion of

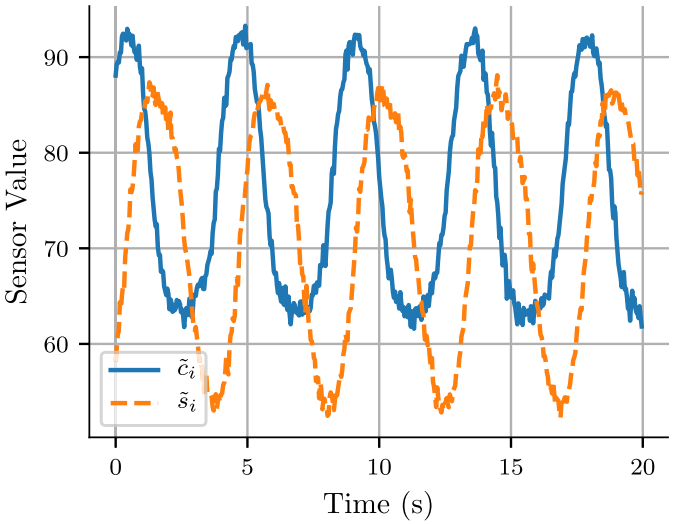

Fig. 5. Type II-A sample waveforms.

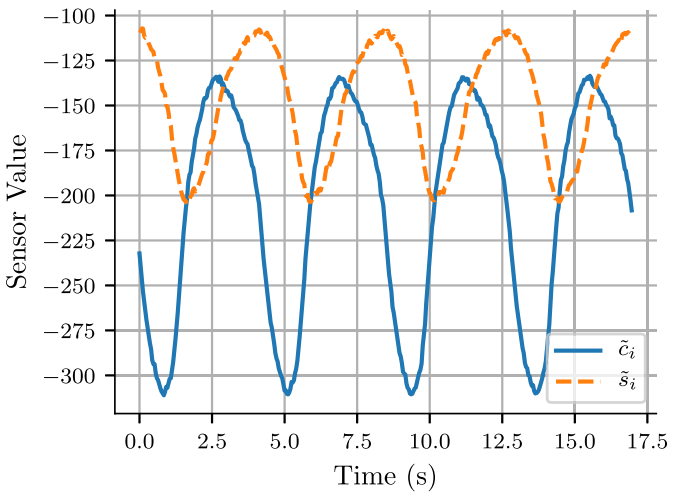

Fig. 6. Type II-B sample waveforms.

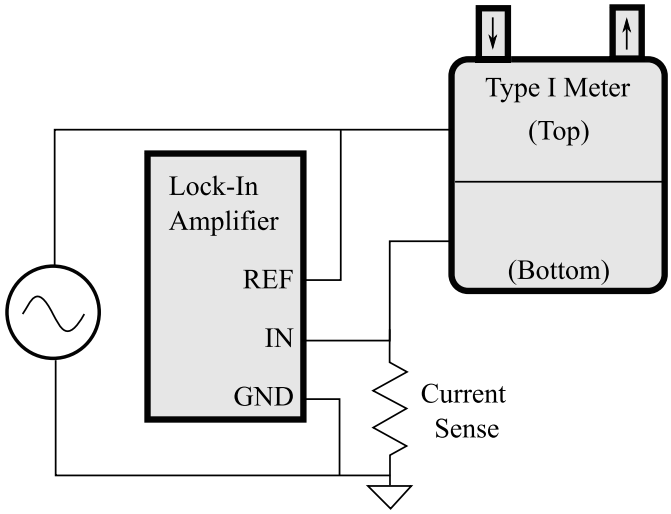

Fig. 7. Type I permittivity measurement schematic.

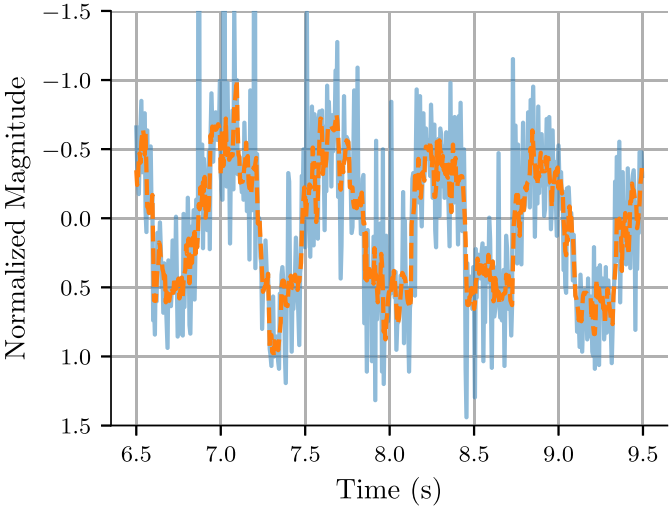

Fig. 8. Type I permittivity measurement sample waveforms.

bellow or flag rod becomes impeded on one side, the negative frequency content of the signal will increase as the measured signals move out of quadrature.

B. Permittivity Sensor and Measurement Setup

To generate the electric field probe for measuring the effective permeability of the Type I meter, electrically conductive probes were soldered to the top and bottom halves of the MB. A signal generator was used to apply a 900 kHz sinusoidal wave across the meter and a current sense, 10 Ω, resistor, as shown in Fig. 7. The SNR of the produced voltage across the current sense resistor is so small that an EG&G Model 5302 Lock-In Amplifier (LIA) was used to measure its magnitude. The output of the LIA was fed into an oscilloscope for data collection purposes.

Even with the LIA to improve SNR, the output was heavily corrupted by noise. A six-point 0.5σ Hampel filter was used to further improve the SNR. Fig. 8 shows a unfiltered and filtered sample waveform, which was normalized to have zero offset and a unity amplitude.

C. Input Preprocessing

Removing field dc bias and scaling the non-unity amplitudes, inherent to both sensing approaches described above, are the first critical steps to reducing errors and producing initial rotation angle estimates. These characteristics may be compensated for, to a first approximation, by measuring the extremes of the field over a rotation. This approach is susceptible to noise and strong non-linearities [18]. Other approaches are available for compensating these parameters, but many rely on reference signals for computing compensation factors which are not available when retrofitting presently-installed meters [3]. To eliminate the need for a reference an angle estimate may be used, as long as the compensation method is stable and converges to unbiased and optimal compensation parameters.

1) Magnetic Field Sensing: For compensating the quadratic signals produced by the magnetic field measurements, we have chosen the Harmonic Error Correction (HEC) method, which estimates sinusoidal amplitude and offset parameters for each orthogonal component using an `arctan2`-based angle estimate and a nonlinear observer [19]. Each non-linear observer

has two adjustable parameters, λ_o and λ_a, which may be used for tuning the method to achieve optimal transient performance while reducing introduced noise. This method features stable and fast convergence with low computational and memory requirements, as well as stability during low and no flow periods of operation, so long as the adjustable observer parameters remain below a stability threshold.

When given the measured quadrature signals, it will produce compensated waveforms $c_i[n]$ and $s_i[n]$ for the leading and lagging quadrature component, respectively, which may be combined into an analytic signal $z_i[n] = c_i[n] + js_i[n]$

2) Permittivity Sensing: Due to the very low SNR of the measured changes in permittivity of the internals of the MB, a six-point 0.5σ Hampel filter is first applied to the signal. Since the HEC method cannot be used without an angle estimate, the signal is compensated using the first approximation approach that tracks the extremes of the field. This compensation method will likely fail in the presence of large transient changes in permittivity created by, e.g., exposure of the exterior of the MB to precipitation, but serves as a proof of concept.

IV. Flow Rate Estimation

The position of the bellows in a BDNG corresponds directly to the phase of the sensed field. The gradient of this phase corresponds to the instantaneous frequency (IF) of the field and therefore the speed of the mechanical motion of the meter. Thus, the IF linearly relates to the flow rate of gas through the meter by a scaling factor F, which may be found using the relation between the meter's cyclic volume and field rotation rate as described in Section II.

For field measurement resulting in quadrature signals, the compensated pair of sinusoids, $(c_i[n], s_i[n])$, may be used to estimate the field's phase and IF. For a single field measurement, just $c_i[n]$ may be used. IF estimates may be generated by taking the gradient of the phase estimate, but added noise from the gradient generally requires more advanced techniques to generate clean estimates [20], [21].

This section describes a digital quadrature phase-locked loop (DQPLL) method using quadrature signals that extracts the phase from the fundamental harmonic present in the measured magnetic field. Higher and lower-order harmonics that are present in the field are modulated on top of the phase estimate, and therefore IF estimate, when using this method and so a post-processing time-varying moving average filter (TVMAF) is introduced. Furthermore, we describe a Continuous Wavelet Transform (CWT) based method for estimating flow rate from a single sinusoid and for generating a reference signal to compare against the results of the DQPLL for quadrature signals.

A. Digital Quadrature Phase-Locked Loop Estimator

Following previous work in sinusoidal-type encoder estimation using phase-locked loops [3], [22]–[24], a DQPLL was used to estimate and track the phase and IF of a quadrature signal pair.

As shown in Fig. 9, this DQPLL is composed of a quadrature phase detector (QPD), proportional-integral loop filter

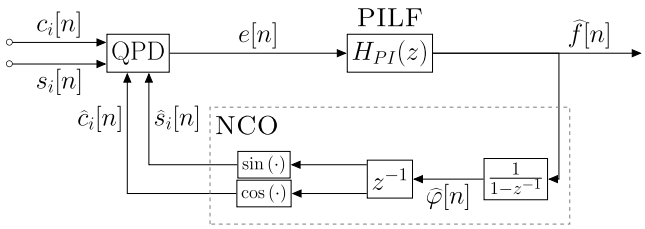

Fig. 9. Digital quadrature phase-locked loop block diagram.

(PILF), and a digital numerically-controlled oscillator (NCO). The QPD estimates the phase difference of the input signals and NCO output by

$$e[n] = s_i[n]\cos(\widehat{\varphi}[n]) - c_i[n]\sin(\widehat{\varphi}[n]). \tag{1}$$

This error signal is then passed through a PILF with parameters K_P and K_I and transfer function

$$H_{PI}(z) = \widehat{f}[n]/e[n] = K_P + K_I/(1 - z^{-1}). \tag{2}$$

When locked, the output of the PILF produces an IF estimate $\widehat{f}[n]$ that is integrated in the NCO to generate a phase estimate $\widehat{\varphi}[n]$. The phase estimate is then used to generate two quadrature signals that are fed back into the QPD.

The DQPLL's inner filters result in a cleaner frequency estimate than that produced by directly taking the gradient of an angle estimate generated using the `arctan2` function. Tuning K_P and K_I allows a user to more accurately track transients in the IF at the expense of increased estimate noise and overshoot. Since the DQPLL estimation method reduces, but does not remove, extraneous field harmonic induced modulation of the phase and IF, a secondary processing step is needed to improve estimates.

A FIR moving average filter (MAF) with window length W acts like a filter with notches at $\frac{F_s}{W}$ Hz and all higher-order harmonics up to the Nyquist frequency and also as a low-pass filter for removing higher frequency noise. Using the estimates computed in the previous section, a TVMAF can be designed, where the window length at sample n is set by the relation

$$W[n] = 1/(s_f \tilde{f}[n]), \tag{3}$$

where s_f is the appropriate scaling factor between the fundamental component of the field and the lowest order extraneous harmonic and $\tilde{f}[n]$ is a smoothed frequency estimate. By setting the window length to this lowest order harmonic, we reduce the effect of its modulation on top of phase estimates, and all of the harmonic's higher-order multiples. This will induce a time-lag in IF estimates of $F_s/W[n]$ s, which can balloon to infinity for IF estimates of zero, but practical limits on window length can be set to minimize this effect during low-load periods. To accurately set a window length, the frequency estimate $\widehat{f}[n]$ is first passed through a MAF to remove noise and produce $\tilde{f}[n]$.

B. Continuous Wavelet Transform Reference

Previous work by the authors has used the CWT to extract the IF from purely real sinusoids, i.e. non-quadrature sinusoidal data [3]. The CWT can be used to generate a time-frequency representation (TFR) of non-stationary waveforms.

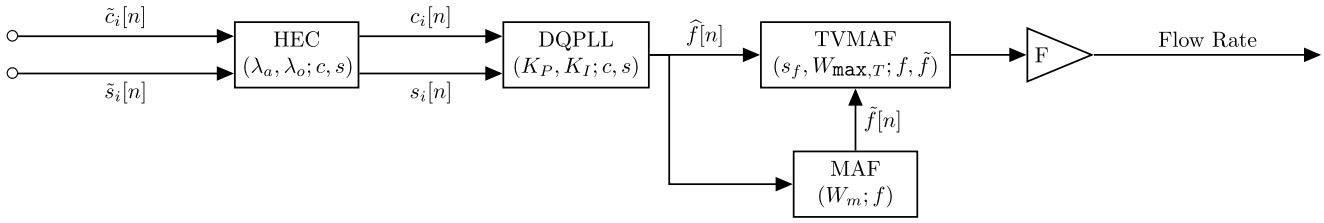

Fig. 10. Magnetic field quadrature signal processing chain overview.

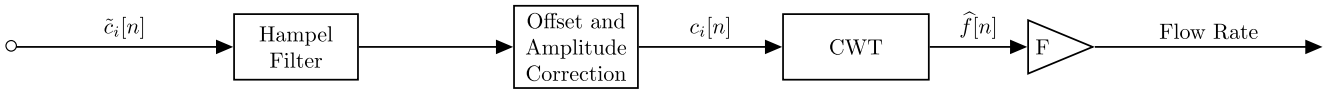

Fig. 11. Permittivity signal processing chain overview.

The choice of wavelet varies the degree of time and frequency localization in the TFR. Nonorthogonal and complex wavelets are best suited for capturing oscillatory behaviors with smooth and continuous variations in parameters [25]. Although this smoothing nature will filter out some transients in our flow, the CWT still serves as a tool for generating accurate flow rate estimates.

A complex Morlet wavelet, chosen as a time/frequency compromise for general flow rate extraction, has the normalized Fourier transform

$$\widehat{\Psi}(s\omega) = (2s)^{1/2}\pi^{1/4}H(s\omega)\exp^{-(s\omega-\omega_0)^2/2}, \tag{4}$$

where ω_0 is a non-dimensional frequency term used to meet wavelet admissibility conditions for the CWT, $H(s\omega)$ is the Heaviside step function, and s is the scale used during the computation of the CWT. Scales can be converted to IF estimates through the relation

$$\widehat{f} = F_s(\omega_0 + \sqrt{2+\omega_0^2})/(4\pi s). \tag{5}$$

The relation shows that one would need an infinite scale to emulate frequencies down to dc, limiting our minimum detectable IF. However, the working range and resolution for the generated TFR can be arbitrarily selected at the cost of increased computational burden. Since the CWT relies on convolving the wavelet with the signal, our implementation uses the Fast Fourier Transform (FFT) and its inverse to improve computational efficiency.

Due to the nature of the CWT process, the harmonics that result in the modulation of the IF estimate from the DQPLL are separated in the TFR. This results in an IF estimate that does not contain this extraneous modulation.

V. Experimental Results

For experimental verification, loads and transients were applied downstream from BDNG meters while either a magnetic field or permittivity was sensed. An overview of the entire magnetic field quadrature signal processing and estimation chain is shown in Fig. 10. An overview of the simpler permittivity signal processing chain is shown in Fig. 11. Both signal processing chains were entirely implemented in `Python` with heavy use of the scientific computing library, `scipy` [26].

TABLE I
Signal Processing and Estimation Parameters

	Meter Type		
	I	II-A	II-B
λ_a	0.005	0.005	0.005
λ_o	0.002	0.005	0.005
K_P	0.01	0.01	0.005
K_I	5×10^{-5}	5×10^{-5}	12.5×10^{-6}
W_m	$10F_s$	$5F_s$	$15F_s$
s_f	0.5	1	1
$W_{\max,T}$	$10F_s$	$10F_s$	$10F_s$
F ($\mathrm{dm^3\,min^{-1}\,Hz^{-1}}$)	35.68	187.5	212.38

A. Magnetic Field Sensing

The parameters for each component in the quadrature signal processing chain can be found in Table I for each meter type. The parameters were chosen based on the expected ranges of flow rates in the experimental setup and would likely need adjustment for different meters and applications. In particular, the parameters associated with the DQPLL dictate the stability and transient performance of the system. Note that the scaling factor at the end of the chain, F, for the Type I meter will be doubled in the electrostatic case because the magnetic coupler's field traverses two sinusoidal periods for every cycle of the body. Estimated flow rates from the proposed signal processing chain compared against the CWT-based reference and $c_i[n]$ are shown in Fig. 12, 13, and 14. Reference data for these figures was generated with a SFM3400 airflow sensor placed in series with the meters [27]. They demonstrated no steady state bias, reasonable transient performance, and reduced extraneous harmonic modulation. The proposed method was stable and tracked the flow rate across the entire range of flow rates tested.

B. Permittivity Sensing

Estimated flow rates from the proposed permittivity sensing chain are shown in Fig. 15. As a reference, the periods of the

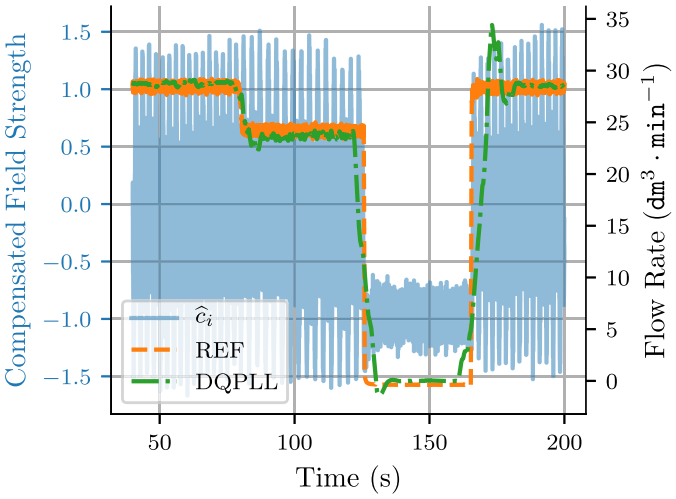

Fig. 12. Type I flow rate extraction.

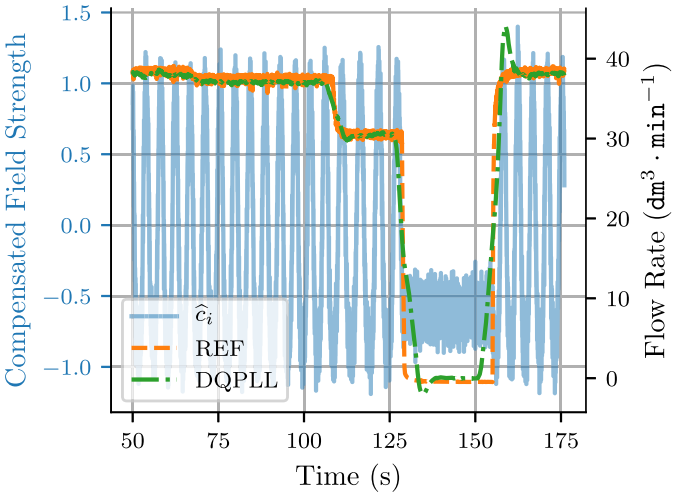

Fig. 13. Type II-A flow rate extraction.

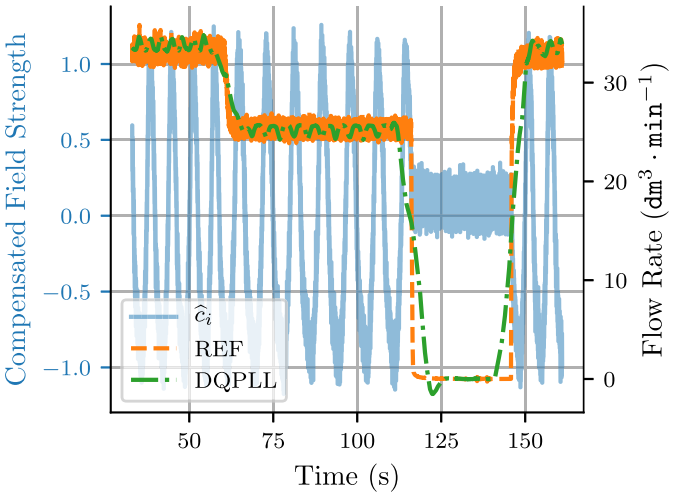

Fig. 14. Type II-B flow rate extraction.

waveform over the measurement period where computed and averaged to generate an IF estimate. The rate was accurately tracked. Permittivity sensing proved highly susceptible to other dielectric events around the meter. For example, touching the meter casing adds a significant dielectric change from the

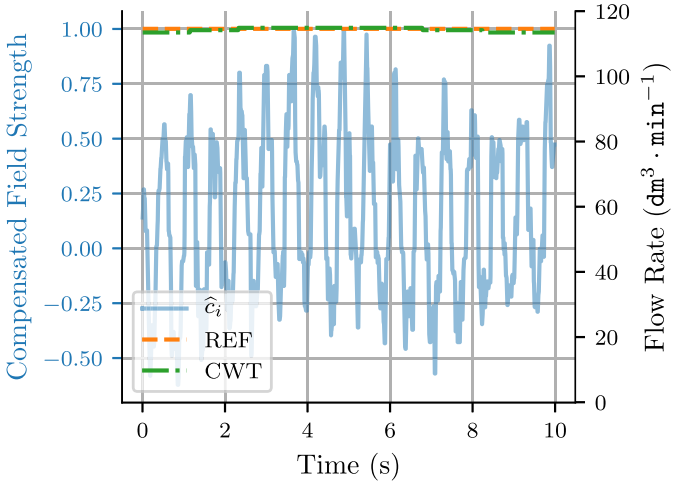

Fig. 15. Type I permittivity flow rate extraction.

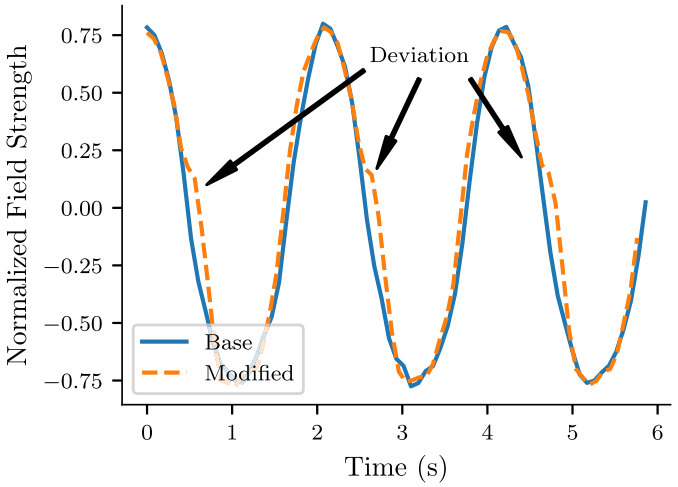

Fig. 16. Compensated measured field on modification-side sensor from a base meter and a modified Type II-A meter.

human contact. The change can be an opportunity, but must be managed. Signal processing is suppressed for very large changes in the permittivity sensing to reject disturbances like touch contacts from affecting flow estimation. However, these changes can also be used to track a persons interaction or interference with the meter mechanism or gas system.

C. Diagnostic Capability Demonstration

A Type II-A BDNG meter was put into a faulty state by weakening the link between a flag rod and one of the bellows. The modification is intended to emulate a meter in the field that may have been exposed to high temperatures, pressures, or shocks. Qualitatively, the modified meter continued to record gas flow but exhibited a more noticeable vibration and jitter in totalizer gauges than the original meter. This manifested itself as a cyclical deviation in the measured field on the side of the meter in which the modification was performed, as can be seen in Fig. 16. In the frequency domain, the modification led to changes in the energy distribution between spatial harmonics in the field, particularly between the second and third harmonics as shown in Fig. 17. With further signal processing and time- or harmonic-based diagnosis techniques,

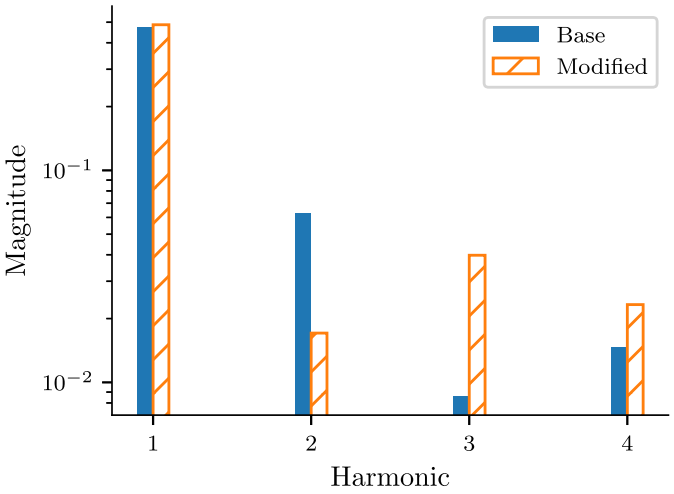

Fig. 17. Harmonic content of samples from a base meter and a modified Type II-A meter.

these signatures in the measured data may thus be further exploited to seek diagnostic value.

VI. Discussion

Using an Intel ®Core i7-7600 CPU running at 2.8 GHz, all signal processing and estimation chain computations took at least an order of magnitude less time to process than overall length of the sample data set, demonstrating their feasibility in real-time applications. Furthermore, the quadrature signal chain consists entirely of simple addition, multiplication, and trigonometric function operations, all of which are well suited for modern embedded microcontroller and DSP architectures. The permittivity based flow rate signal processing chain relies on the FFT which is similarly well suited for modern architectures. Furthermore, the necessary sample rates to capture high quality flow rate data are relatively low and so the methods are well suited to real-time embedded applications.

The TVMAF used in this work is critical for producing human-readable flow rates. However, it contributes the most to transient suppression and computational burden in the quadrature signal chain. In particular, transients down to or up from very low flow-rates are heavily smoothed due to the very large MAF window size needed. For non intrusive load monitoring applications using harmonic analysis or correlation functions for load disaggregation, the final TVMAF step may reduced or removed to improve transient performance.

With regards to low-flow rate performance, the Type I meter is accurate down to 0.66 $\mathrm{dm}^3\,\mathrm{min}^{-1}$ and the Type II-A meter is accurate down to 11.6 $\mathrm{dm}^3\,\mathrm{min}^{-1}$. These low-flow rates would require longer windows for smoothing operations and further tuning.

At the sampling rates used in this work, a magnetic sensor and microcontroller pair could extract and process the data as shown here, continuously, for an estimated power draw of well less than 0.5 W. For the permittivity sensing approach, microcontroller integrated capacitive sensing hardware could replace the instruments used in this work and would offer similarly low power consumption.

The permittivity sensing results show great promise for using electric fields to probe mechanical motion of dielectric internal structures. The electric field strengths that are most easily created and applied to the mechanical mechanism, in this case, would typically be voltage limited and sensitive to interference from neighboring materials with relatively high dielectric constant and external polarizable materials, e.g., contact with a human hand, which can induce transients in the measurements. Therefore, the SNR of the measured signal with this approach is relatively low compared to the magnetic approaches, where permanent magnets provide very substantial probe field strengths. The transients can be distinguished in amplitude from the probe of the meter mechanism. The dielectric approach therefore offers pluses and minuses. Dielectric probing permits nonintrusive monitoring of "plastic" mechanical mechanisms. While this probing may be disturbed by external permeable material interactions, the sensitivity to these interactions may also serve as a warning of tampering or changes in the overall system environment. More generally, the choice of probe field also must consider the relative safety merits of electric versus magnetic fields around working fluids like gas or water. In particular, no clear standard regarding the use of voltages in the presence of the volatile compounds found in natural gas was found, likely due to the difficult to quantify ignition risks.

VII. Conclusion

This article presents a methodology and example systems for nonintrusively retrofitting BDNG meters for flow rate extraction. Approaches for nonintrusive retrofit can use either an internally available field source or an externally applied field. Disturbances and changes in field distribution serve as "passive probes" or tell-tale indicators revealing the operation of the underlying mechanism. Among other possibilities, signal processing can be used to extract flow rate information from this passive probing. Our work presents an approach for low-cost and real-time applicable flow rate extraction without invasive modification or complex image-processing hardware, as required by previous work.

More generally, any moving mechanical structure, including devices constructed with either permeable (magnetic) or dielectric (plastic) materials, can be probed using variants of the techniques described in this paper. These probes can provide usage tracking and also indicated signatures associated with diagnostic conditions as components wear or break.

References

[1] J. Marais, R. Malekian, N. Ye, and R. Wang, "A review of the topologies used in smart water meter networks: A wireless sensor network application," *J. Sensors*, vol. 2016, pp. 1–12, Oct. 2016.

[2] C. Schantz, J. Donnal, B. Sennett, M. Gillman, S. Müller, and S. Leeb, "Water nonintrusive load monitoring," *IEEE Sensors J.*, vol. 15, no. 4, pp. 2177–2185, Apr. 2015.

[3] E. A. Ponce, S. B. Leeb, and P. A. Lindahl, "Know the flow: Non-contact magnetic flow rate sensing for water meters," *IEEE Sensors J.*, vol. 21, no. 1, pp. 802–811, Jan. 2021, doi: 10.1109/JSEN.2020.3014843.

[4] S. Yamagami, H. Nakamura, and A. Meier, "Non-intrusive submetering of residential gas appliances," Lawrence Berkeley Nat. Lab., Berkeley, CA, USA, Tech. Rep. LBNL-38982, CONF-9608106-7, Aug. 1996. Accessed: May 21, 2019. [Online]. Available: https://www.osti.gov/biblio/418458

[5] M. Tewolde and J. P. Longtin, "High-resolution meter reading system for gas utility meter," in *Proc. IEEE Sensors*, Nov. 2010, pp. 849–852, doi: 10.1109/ICSENS.2010.5690859.
[6] M. Tewolde, J. C. Fritch, and J. P. Longtin, "High-resolution meter reading technique for appliance gas usage monitoring for the smart grid," in *Proc. 8th Int. Conf. Expo. Emerg. Technol. Smarter World*, Nov. 2011, pp. 1–6, doi: 10.1109/CEWIT.2011.6135876.
[7] M. Tewolde, J. C. Fritch, and J. P. Longtin, "Design of a low-cost, high-resolution retrofit module for residential natural gas meters," *Appl. Thermal Eng.*, vol. 75, pp. 357–365, Jan. 2015, doi: 10.1016/j.applthermaleng.2014.09.041.
[8] E. Moniz, "The future of natural gas: An interdisciplinary MIT study," in *MIT Energy Initiative*. Cambridge, MA, USA: MIT, 2011.
[9] B. Travis, M. Dubey, and J. Sauer, "Neural networks to locate and quantify fugitive natural gas leaks for a MIR detection system," *Atmos. Environ., X*, vol. 8, Dec. 2020, Art. no. 100092, doi: 10.1016/j.aeaoa.2020.100092.
[10] J. Thomson, "Fundamental principles of diaphragm meters," in *Proc. 70th Int. School Hydrocarbon Meas.*, 1995, pp. 28–32.
[11] M. S. Crainic, "A shorth history of diaphragm gas meters part ii evolution of modern diaphragm gas meters," in *Proc. Installations Buildings Ambiental Comfort Conf. 21th Timisoara Romania*, Apr. 2010, pp. 189–215.
[12] *Atmos Diaphragm Gas Meter*, Zenner Int. GmbH & Co. KG, Saarbrücken, Germany. [Online]. Available: https://pim.zenner.com/wp-content/uploads/documents/catalogues/EN/KT_GAS_EN.pdf
[13] V. T. Nguyen and T.-F. Lu, "Analytical expression of the magnetic field created by a permanent magnet with diametrical magnetization," *Progr. Electromagn. Res. C*, vol. 87, pp. 163–174, 2018, doi: 10.2528/PIERC18073001.
[14] *AC-250*, Honeywell Elster, Nebraska City, NE, USA, 2008. [Online]. Available: https://www.elster-americanmeter.com/assets/products/products_elster_files/EAM-DS3535.pdf
[15] *R-275 Diaphragm Gas Meters*, Sensus, DuBois, PA, USA. [Online]. Available: https://sensus.com/products/r-275-r-315/
[16] *MLX90393 Triaxis Magnetic Node*, document MLX90393 datasheet, Melexis, Nov. 2014.
[17] Z. Zhang, C. Xiao, K. Yin, and H. Yan, "A magnetic field correction method for the non-ideally placed 3-axial magnetometer sensor," in *Proc. Int. Conf. Measuring Technol. Mechatronics Autom.*, vol. 1, Mar. 2010, pp. 130–133.
[18] S. Balemi, "Automatic calibration of sinusoidal encoder signals," *IFAC Proc.*, vol. 38, pp. 68–73, Jul. 2005.
[19] C. Albrecht, J. Klöck, O. Martens, and W. Schumacher, "Online estimation and correction of systematic encoder line errors," *Machines*, vol. 5, no. 1, p. 1, Jan. 2017, doi: 10.3390/machines5010001.
[20] B. Boashash, "Estimating and interpreting the instantaneous frequency of a signal. I. Fundamentals," *Proc. IEEE*, vol. 80, no. 4, pp. 520–538, Apr. 1992.
[21] B. Boashash, "Estimating and interpreting the instantaneous frequency of a signal. II. Algorithms and applications," *Proc. IEEE*, vol. 80, no. 4, pp. 540–568, Apr. 1992.
[22] T. Emura and L. Wang, "A high-resolution interpolator for incremental encoders based on the quadrature PLL method," *IEEE Trans. Ind. Electron.*, vol. 47, no. 1, pp. 84–90, Feb. 2000.
[23] H. V. Hoang and J. W. Jeon, "Signal compensation and extraction of high resolution position for sinusoidal magnetic encoders," in *Proc. Int. Conf. Control, Autom. Syst.*, Oct. 2007, pp. 1368–1373.
[24] H. Tue Le, H. Van Hoang, and J. Wook Jeon, "Efficient method for correction and interpolation signal of magnetic encoders," in *Proc. 6th IEEE Int. Conf. Ind. Informat.*, Jul. 2008, pp. 1383–1388.
[25] C. Torrence and G. P. Compo, "A practical guide to wavelet analysis," *Bull. Amer. Meteorolog. Soc.*, vol. 79, no. 3, pp. 61–78, Jan. 1998.
[26] P. Virtanen *et al.*, "SciPy 1.0-Fundamental algorithms for scientific computing in Python," 2019, *arXiv:1907.10121*.
[27] *Data Sheet—SFM3400*, Sensirion, Staefa ZH, Switzerland, May 2017. [Online]. Available: https://sensirion.com/media/documents/70FC8320/616687F2/Sensirion_Mass_Flow_Meters_SFM3200_Datasheet.pdf

Eric A. Ponce received the B.S. and M.Eng. degrees from the Massachusetts Institute of Technology in 2017 and 2019, respectively, where he is currently pursuing the Ph.D. degree.

Steven B. Leeb (Fellow, IEEE) received the Ph.D. degree from the Massachusetts Institute of Technology in 1993. He has served as a Commissioned Officer for the U.S. Air Force Reserve, and he has been a member of the MIT faculty at the Department of Electrical Engineering and Computer Science since 1993. He also holds a joint appointment with the MIT's Department of Mechanical Engineering. He is the author or coauthor of over 150 publications and holds 20 U.S. patents in the fields of electromechanics and power electronics.